

Figure 4 Column capacity varying with temperature for interior gravity column supporting the 6th floor (W12x58) (a) column capacity compared with column load and prediction temperature for failure, (b) column capacity compared with mean column load throughout building with 95% confidence interval for failure

SUMMARY

The fifth floor of a ten-story steel-frame office building with exterior MRFs was subjected to a full story fire while varying FRR on the structural members. Utilization ratios of the interior gravity columns showed that the fifth floor was representative of a typical story in the building. Three different FRR options were simulated with a full-story fire: (1) design FRR on all structural members, (2) columns protected with 2hr FRR, beams and girders protected with design FRR, and (3) columns protected with 2hr FRR, secondary beams unprotected, and girders protected with design FRR. The results of these three simulations showed that when all structural members are protected with the design FRR, the gravity columns will fail first causing collapse of the building. When the columns are protected for 2hr FRR, and the secondary beams are left unprotected, large midspan deflections of the floor system are observed; however no collapse of the building was observed. When both the beams and girders are protected for the design FRR, and the columns are protected for 2hr FRR, there is no collapse in the building due to a full-story fire.

FUTURE WORK

The results of the full-story fire scenarios presented in this paper highlight the need for more large-scale experimental and numerical research on the collapse mechanisms of steel-frame buildings. The findings presented here apply to steel-frame buildings with exterior MRFs, however, in the U.S. building inventory includes braced frame buildings as well. These buildings should be evaluated for their behavior in fire. These frames do not include very large cross sections for beams and columns as MRF buildings do, and therefore will behave differently during a fire.

The building collapse simulated by the 3D FEM models presented in this paper are limited by the simplified modeling techniques implemented. The composite beam behavior was not modeled through force-slip behavior as defined by Zhao and Kruppa (1997) but rather through rigid links between the steel beam and concrete on metal deck. Therefore the behavior of the secondary unprotected beams could be simulated in a more realistic way to adequately model the behavior of composite beams during fires.

The performance of the two buildings evaluated in this paper examined the effect of only fire on the building. Future work should consider the effect of multi-hazards on these buildings (i.e. fire following earthquake). For instance, after an earthquake plasticity has developed in the steel members of the lateral system or the reinforced concrete core wall may be cracked. These two instances can decrease the available strength and stiffness of the building when a fire starts causing the survival time of the building to decrease.

REFERENCES

- Abaqus/Standard Version 6.13 User's Manual. (2013). Providence, RI.
- Agarwal, A. (2011). Stability Behavior of Steel Building Structures in Fire Conditions. (Doctor of Philosophy, Civil Engineering). West Lafayette, IN: Purdue University.
- Agarwal, A., & Varma, A. H. (2014). Fire induced progressive collapse of steel building structures: The role of interior gravity columns. *Engineering Structures*, 58, 129-140.
- Agarwal, A., Selden, K. L., & Varma, A. H. (2014). Stability Behavior of Steel Building Structures in Fire Conditions: Role of Composite Floor Systems with Shear-Tab Connections. *Journal of Structural Fire Engineering*, 5(2), 77-96.
- American Institute of Steel Construction, Inc. (2010). Specification for Structural Steel Buildings, ANSI/AISC 360-10. Chicago, IL: AISC.
- American Society of Civil Engineers. (2010). Minimum Design Loads for Buildings and Other Structures (ASCE 7-10). Reston, VA: ASCE.
- Cedeno, G., Varma, A. H., & Agarwal, A. (2009). Behavior of Floor Systems under Realistic Fire Loading. *Proceedings of ASCE Structures Congress*. Orlando, FL.
- European Committee for Standardization (CEN). (2002). Eurocode 1: Actions on Structures, Part 1.2: General Actions - Actions on Structures Exposed to Fire.
- European Committee for Standardization (CEN). (2005). Eurocode 4: Design of composite steel and concrete structures, Part 1.2: General Rules - Structural Fire Design.
- Fischer, E. C. (2015). Behavior of Simple (Shear) Connections in Steel-Frame Buildings During Fire. West Lafayette, IN: Lyles School of Civil Engineering, Purdue University.
- Fischer, E. C., Agarwal, A., & Varma, A. H. (In Review). Fire induced progressive collapse of steel-framed buildings: Compartment Fires. *Journal of Constructional Steel Research*.
- IBC. (2009). International Building Code. Falls Church, VA, VA: International Code Council Inc.

- Jiang, Y., Kotsovinos, P., Usmani, A., Rein, G., & Stern-Gottfried, J. (2013). Numerical investigation of thermal response of a composite structure in horizontally travelling fires using OpenSees. *Procedia Engineering*, 62, 736-744.
- Luecke, W. E., Gross, J. L., & McColskey, J. D. (2014). High-temperature tensile, constitutive models for structural steel in fire. *AISC Engineering Journal*.
- Phan, L. T., Gross, J. L., & McAllister, T. P. (2010). *Best Practice Guidelines for Structural Fire Resistance of Concrete and Steel Buildings (NIST TN-1681)*. Gaithersburg, MD: National Institute of Standards and Technology.
- Ruddy, J. L., Marlo, J. P., Loanneides, S. A., & Alfawakhiri, F. (2003). *Design Guide 19: Fire Resistance of Structural Steel Framing*. Chicago, IL: American Institute of Steel Construction.
- Sarraj, M., Burgess, I. W., Davison, J. B., & Plank, R. J. (2007). Finite element modeling of steel fin plate connections in fire. *Fire Safety Journal*, 42, 408-415.
- Takagi, J., & Deierlein, G. G. (2007). Strength Design Criteria for Steel members at Elevated Temperatures. *Journal of Construction Steel Research*, 63(8), 1036-1050.
- UL Directory. (2004). *Fire Resistance Directory*. Northbrook, IL: Underwriters Laboratories, Inc.
- Zhao, B., & Kruppa, J. (1997). Fire resistance of composite slabs with profiled steel steel and of composite steel concrete beams, Part 2: Composite Beams. Luxembourg: European Commission.

Integrated Fire-Structure Simulation Methodology for Predicting the Behavior of Structures in Realistic Fires

Chao Zhang¹

¹National Institute of Standards and Technology, Gaithersburg, MD; Tongji Univ., Shanghai, China. E-mail: chao.zhang@nist.gov

Abstract

This paper presents the numerical modeling of a test on a 6-meter-long steel W-section beam subjected to combined structural load and localized fire. An integrated fire-structure simulation approach was successfully applied to model the fire-thermal-structural behavior of the beam specimen. The difference ratios between the predicted and measured values for failure time, failure temperature and failure load can be as small as 0.7% (0.2 min), 2.9% (19 °C) and 9% (9 kN), respectively. In this paper, failure temperature is defined as the maximum temperature in the beam specimen at the onset of failure. Detailed description of the numerical models was presented. The study might serve as a validation case of the integrated fire-structure simulation approach which could be used in structural fire engineering design.

INTRODUCTION

Over the past three decades, a number of fire tests (Kirby 2000; Kodur 1999; Choe et al. 2011; Morovat 2014) and numerous analytical studies (Bailey 2001; Usmani et al. 2001; Yin and Wang 2005; Zhang and Usmani 2015; Jeffers and Sotelino 2012) have been conducted in order to develop new approaches for structural fire safety design. Most of those studies used the standard fire or simulated compartment fires, and assumed uniform heating conditions. Modern buildings usually include large enclosures, e.g., sport stadiums, transportation terminals, atria and open plan compartments. The fires in large enclosure are characterized as localized fires in which the heating conditions are non-uniform (Zhang and Li 2012). Because of thermal gradients, the behaviors of structures under uniform and non-uniform heating conditions might be significantly different (Zhang et al. 2013a; Zhang et al. 2015). As a result, the behavior of structures exposed to localized fire should be investigated to ensure structural fire safety in large enclosures. To date, some numerical studies using simple fire models, e.g. SFPE correlations (Lattimer 2002), have been conducted to investigate the behavior of steel beams exposed to localized fire (Jeffers and Sotelino 2012; Zhang et al. 2013b). While those studies are valuable to understand the effect of thermal gradient on structural behavior, experimental data and sophisticated fire models are needed to adequately predict the response of structures exposed to localized fire.

Recently, there has been increased interest in the community of structural fire engineering to study the application of the Fire Dynamics Simulator (FDS) for structural fire safety design (Zhang et al. 2016c). FDS is an open source LES (large-eddy simulation) code, developed for fire related simulations (McGrattan et al. 2013). It has been used in fire engineering for modeling the gas phase environments

(temperature, heat flux, velocity, species concentrations, etc.) in fires. Fire-structure interface tools for transferring data from FDS to particular FEM (Finite Element Method) codes (such as ANSYS, ABAQUS, SAFIR) have been developed. However, there is a lack of investigation on the applicability of FDS for structural fire analysis, mainly due to the limited available test data on structures exposed to realistic fire scenarios.

The National Institute of Standards and Technology recently added a unique facility named the National Fire Research Laboratory (NFRL), which intends to serve research needs of studying the response of real-scale structural systems to realistic fires as well as other fire research topics such as advanced firefighting technologies, engineered fire safety, material flammability reduction and wildland-urban interface fire research (Bundy et al. 2016). The unique facility enables large-scale experiments using fires up to 20 MW and will contribute to the technical basis for performance-based design methodologies for structures exposed to fire. This paper presents the detailed numerical study of a structural test on a 6 m long steel W-section beam exposed to localized fire conducted at the NFRL. A FDS-FEM (finite element method) approach is used to predict the fire-thermal-structural behaviors in the test.

ELEVATED TEMPERATURE MATERIAL MODEL

Thermal properties for structural steel specified in the Eurocode (BSI 2005) were used. The density of the structural steel was 7850 kg/m^3 . Fig.1 plots the temperature-independent (dash line) and -dependent (solid line) specific heat and thermal conductivity.

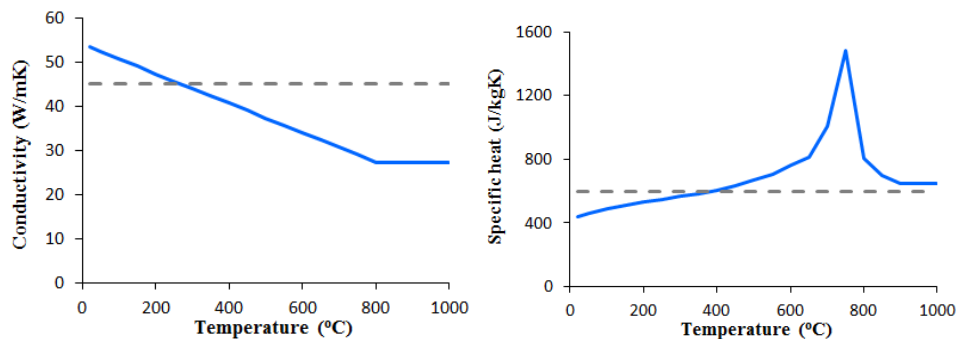


Figure 1 Thermal conductivity (left) and specific heat (right) of structural steel

The thermal expansion coefficient for structural steel recommended by NIST TN 1681 (Phan et al. 2010) was used,

$$\alpha_s = 1.17 \times 10^{-5} + 1.34 \times 10^{-8} T - 9.7 \times 10^{-12} T^2 + 1.67 \times 10^{-16} T^3 \quad (1)$$

The stress-strain model for structural steel developed by Luecke et al. (2011) was used,

$$\sigma = \begin{cases} \varepsilon E_T & (\varepsilon \leq \frac{f_{yT}}{E_T}) \\ f_{yT} + (k_3 - k_4 f_{y20}) \exp\left[-\left(\frac{T}{k_2}\right)^{k_1}\right] \left(\varepsilon - \frac{f_{yT}}{E_T}\right)^n & (\varepsilon > \frac{f_{yT}}{E_T}) \end{cases} \quad (2)$$

with $k_1 = 7.820$, $k_2 = 540$ °C, $k_3 = 1006$ MPa, $k_4 = 0.759$, and $n = 0.503$. σ and ε are stress and strain. The elastic modulus and yield strength at elevated temperature are given by

$$\frac{E_T}{E_{20}} = \exp\left[-\frac{1}{2}\left(\frac{T-20}{639}\right)^{3.768} - \frac{1}{2}\left(\frac{T-20}{1650}\right)\right] \quad (3)$$

and

$$\frac{f_{yT}}{f_{y20}} = 0.09 + 0.91 \exp\left[-\frac{1}{2}\left(\frac{T-20}{588}\right)^{7.514} - \frac{1}{2}\left(\frac{T-20}{676}\right)\right] \quad (4)$$

respectively. Where E_{20} and E_T are elastic modulus of steel at room and elevated temperatures, respectively; and f_{y20} and f_{yT} are yield strength of steel at room and elevated temperatures, respectively. The constitutive model developed by Luecke et al. (2011) was selected for its better representation of the tensile coupon test data (Choe et al. 2016b).

TEST SETUP

Figure 2 shows schematic diagram of the test setup, composed of the W16x26 beam specimen, reaction frames, and HSS (hollow structural section) loading beams. All the components of reaction frames were designed in accordance with the ANSI/AISC-360-10. The length of the beam specimen was 6.17 m. The beam specimen was simply supported with the bearing-to-bearing length of 5.87 m. The beam specimen was placed at 1.67 m above the strong floor and were loaded by means of two HSS loading beams placed at 1.22 m away from the center of the specimen. The ends of the beam specimen and the regions in contact with the HSS loading beams were laterally and rotationally restrained. The lengths of the HSS loading beams were 6.71 m. The lengths of the cover plates welded to the HSS section were 3.81 m. Two holes were dug on the HSS tube to apply pull force through the high-strength robs. The distances from the holes to the center of the loading beam were 2.74 m. A detailed description of the test setup, instruments and test results can be found in Choe et al. (2016a).

For the structural fire test, the fuel delivery system consists of two natural gas burners with a nominal flame zone of one square meter to provide heat release rate (HRR) up to 1.5 MW. The assembled burner was placed 1 m below the lower flange of the specimen. The method used to determine the heat release rate of the test fire is discussed in another paper (Zhang et al. 2016a) and not presented here for brevity.



Figure 2 Test setup (left) and installation of plate thermometers (right)
AMBIENT TEST SIMULATION

Finite element model

Before the structural fire test, an ambient test was conducted to investigate the load-bearing capacity of the beam specimen. Figs.3 and 4 show the FEM model for the ambient test. The beam specimen and the loading beams were meshed with the four-node structural shell element SHELL181 in ANSYS (2015). The axial displacements (along Z direction in the FE model) of the loading beams were restrained (see ① in Fig. 4). The lateral displacements (along X direction) of the loading beams were restrained at the loading points (see ②). To model the simply supported boundary conditions, the vertical displacements (along Z direction) of the nodes of the lower flange at the support and the lateral displacements (along X direction) of the four corner nodes were restrained (see ③ or ④). At the intersections of the beam specimen and the loading beams, the lateral displacements of the exterior nodes of the stiffener, the four corner nodes of the beam specimen, and the nodes at the bottom of the loading beam were coupled (see ⑤). At the intersection, the vertical displacements (along Y direction) of the nodes of the upper flange of the beam specimen and the nodes of the bottom of the loading beam were also coupled (see ⑥). Concentration forces or displacements were applied along the lines on the top of the loading beams (see ②). Initial geometrical imperfection in the test specimen was measured and the measured amplitude of $L/900$ was applied in the FE model. Here, L is the length of beam specimen. Residual stress was not considered in the FE model.

The steel for the beam specimen was ASTM A572 Gr. 50, for the HSS section was ASTM A500 Gr. B and for the cover plate of the loading beam was ASTM A36. The measured yield strength (f_{y20}) for the steel of the beam specimen was 440 ± 1.15 MPa. Here, the standard uncertainty is estimated based on the certified material test report provided by steel fabricator and assumption of uniform distribution. The numbers following the symbol \pm are the expanded uncertainty with a level of confidence of approximately 95%.

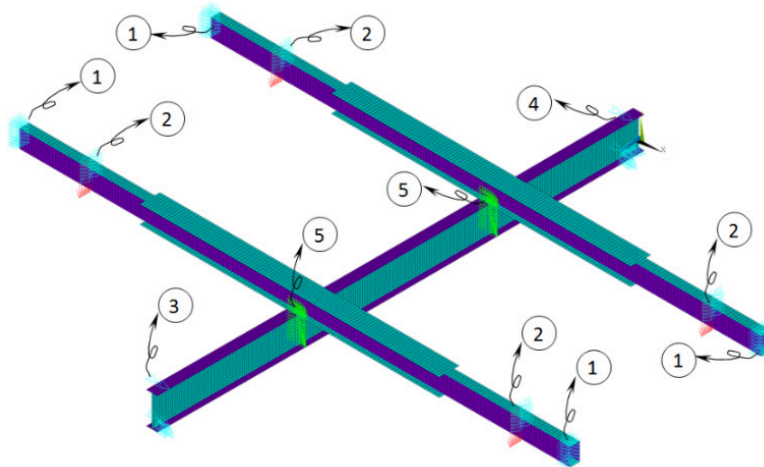


Figure 3 Finite element model for the ambient test

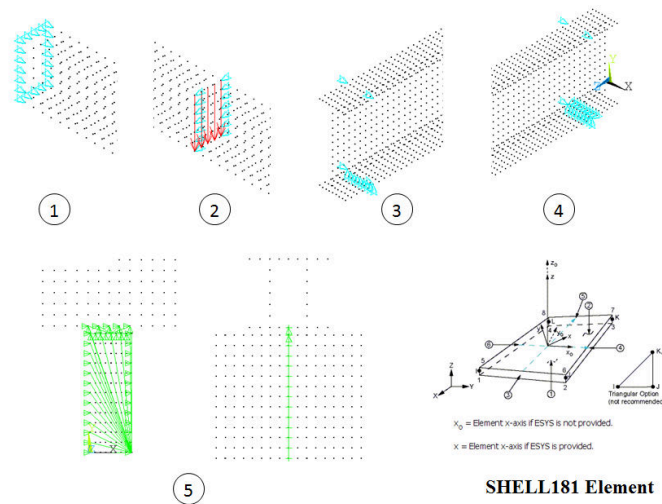


Figure 4 Load and boundary conditions in the finite element model

Results for ambient test

Figure 5 shows the predicted load-displacement curves for the ambient test. The test data are also presented. The beam specimen failed by lateral torsional buckling and the measured maximum reaction force was 146 kN. In FE simulation, a linearly increasing displacement was simultaneously applied at the four load cells (② in Fig.4) and the predicted maximum reaction force was 152 kN.

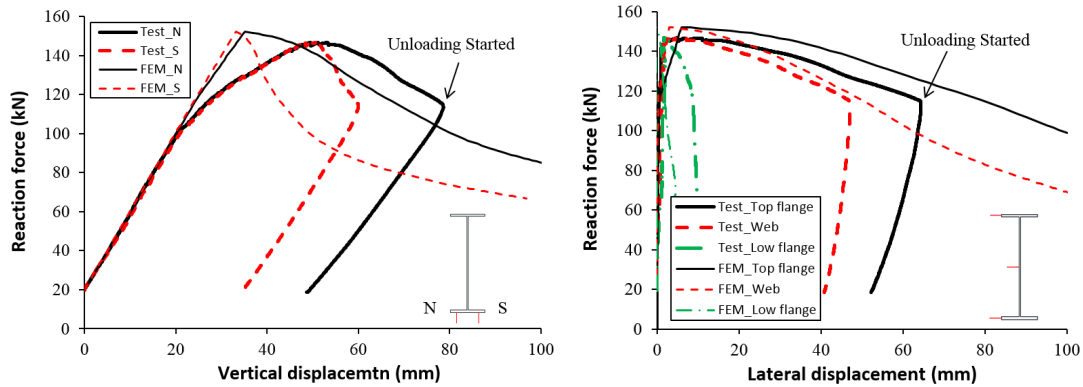


Figure 5 Numerical results against test data for the ambient test.

FIRE DYNAMICS SIMULATION

The FDS code

The LES code FDS (version 6.1.1) was utilized to predict the fire environment in the structural fire test. LES is a technique used to model the dissipative processes (viscosity, thermal conductivity, material diffusivity) that occur at length scales smaller than those that are explicitly resolved on the numerical grid. In FDS, the combustion is based on the mixing-limited, infinitely fast reaction of lumped species, which are reacting scalars that represent mixtures of species. Thermal radiation is computed by solving the radiation transport equation for gray gas using the Finite Volume Method (FVM) on the same grid as the flow solver. FVM is based on a discretization of the integral forms of the conservation equations. It divides the problem domain into a set of discrete control volumes (CVs) and node points are used within these CVs for interpolating appropriate field variables. The governing equations are approximated on one or more rectilinear grids. Obstructions with complex geometries are approximated with groups of prescribed rectangles in FDS. One-dimensional (1D) heat conduction is assumed for solid-phase calculations. Note that a three-dimensional heat conduction feature is under development in FDS (Zhang et al. 2016b).

The concept of adiabatic surface temperature

To achieve a better prediction of solid temperature, the fire-structure one-way coupling simulation approach described in Zhang et al. (2016c) and similarly in Duthinh et al. (2008) has been used in this study. By the approach, the FDS predicted thermal boundary conditions at the exposed surfaces of the beam specimen are mapped into the three-dimensional (3D) heat transfer model in ANSYS to predict the solid (steel) temperatures. The concept of adiabatic surface temperature has been used as the fire-structure interface to transfer thermal boundary condition data from FDS to ANSYS, which is briefly described as follows.

Consider an ideal adiabatic surface exposed to a heating condition, the net heat flux to the surface is by definition zero, and the incident radiative flux to the surface can be calculated by,

$$\dot{q}_{in}'' = \frac{h_{c,AS}(AST - T_g)}{\varepsilon_{AS}} + \sigma AST^4 \quad (5)$$

where AST is the adiabatic surface temperature; ε_{AS} is emissivity of the adiabatic surface; and $h_{c,AS}$ is film coefficient between the adiabatic surface and the surrounding gas; T_g is the surrounding gas temperature; and σ is the Stefan-Boltzmann constant. Accordingly, the net heat flux to a real surface with the same emissivity ($\varepsilon_s = \varepsilon_{AS}$), the same film coefficient ($h_{c,s} = h_{c,AS}$), and exposed to the same heating condition can be calculated by

$$\dot{q}_{net}'' = \varepsilon_s \sigma (AST^4 - T_s^4) + h_c (AST - T_s) \quad (6)$$

Eq. (6) shows that the net heat flux to a surface can be calculated by using a single parameter AST . In practice, the adiabatic surface temperatures of interest can be approximately measured by a plate thermometer. FDS includes an output quantity of adiabatic surface temperature according to the idea proposed by Wickstrom (Wickstrom et al. 2007).

The FDS numerical model

Figure 6 shows the time-history curve of heat release rate of the burner in FDS simulation. The measured heat release rates are also plotted. The uncertainty in the HRR measurements with a nature gas burner is presented in Bryant et al. (2015) and not presented here for brevity. Fig. 7 shows the geometry and mesh of the FDS numerical model. Dimensions of the computational domain were 7.2 m (X) \times 1.2 m (Y) \times 3.6 m (Z). The grid size used is an important numerical parameter in CFD because of its impact on numerical accuracy. Three meshes were considered in this study. For mesh 1, uniform grids of 4 cm were used in the Y and Z directions, and mid-stretched grid was used in the X direction (the smallest grid size was 4 cm.); for mesh 2, uniform grids of 2 cm were used in the Y and Z directions, and mid-stretched grid was used in the X direction (the smallest grid size was 2 cm); and for mesh 3, mid-stretched grids were used in X, Y and Z directions (the smallest grid size was 2 cm). Therefore, the computational domain consisted of 1,555,200 control volumes for mesh 1, 291,600 control volumes for mesh 2 and 388,800 control volumes for mesh 3.

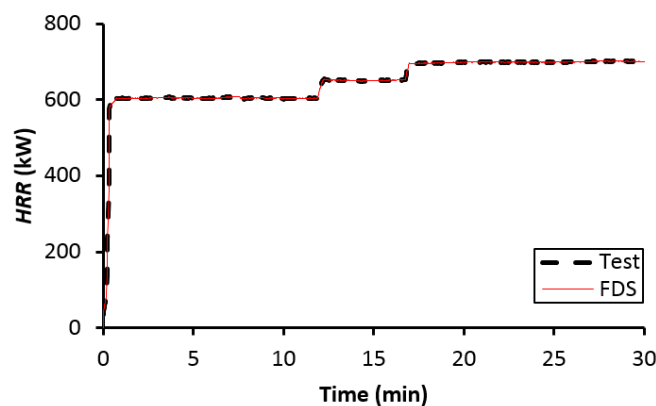


Figure 6 The HRR time-history curve in FDS simulation.